MSc in Photonics

PHOTONICSBCN

Universitat Politècnica de Catalunya (UPC)
Universitat Autònoma de Barcelona (UAB)
Universitat de Barcelona (UB)
Institut de Ciències Fotòniques (ICFO)

http://www.photonicsbcn.eu

Master in Photonics

MASTER THESIS WORK

NONLINEAR OPTICAL PROPERTIES OF ORGANO-METALLIC FILMS

Marina Mariano Juste

Supervised by Dr. Roberto Macovez and Prof. Jordi Martorell, (ICFO)

Presented on date 9th July 2009

Registered at

Escola Tècnica Superior
d'Enginyeria de Telecomunicació de Barcelona

Nonlinear optical properties of organo-metallic films

Marina Mariano Juste

Organic nanostructured photovoltaics group. Institut de Ciències Fotòniques, Mediterranean Technology Park, Av. del Canal Olímpic, Castelldefels 08860 (Barcelona) Spain.

E-mail: `marina.mariano@icfo.es`

Abstract. Joining organic molecules and metallic nanoparticles into coupled heterostructures allows tuning their optical properties and offers novel possibilities for manipulating their emission patterns. This Master Thesis is aimed at probing and understanding the nature of the optical coupling between plasmonic nanoparticles and organic molecules. We carry out second harmonic spectroscopy and interferometry experiments on thin films of the nonlinear dye crystal violet deposited on glass and on top of silver nanoparticles to study the interplay between the resonance of the dye and the plasmon modes of the nanoparticles. We find a small redshift of second harmonic emission from the nanoparticles, while the molecular second harmonic resonance displays a large blueshift of tens of nanometers in the vicinity of the nanoparticles. Across both resonances a characteristic shift of π in the phase of the generated second harmonic light is observed by second harmonic interferometry. To explain our findings, a phenomenological model with two coupled damped anharmonic oscillators is proposed. With the model, we are able to reproduce the main features of the experimental data.

Keywords: Second harmonic generation, nonlinear interferometry, optical coupling, plasmonic nanoparticles, and hybrid metallo-organic structures.

1. Introduction.

The optical properties of metallic nanoparticles and organic materials have been the subject of extensive fundamental and applied research. During the past few years there has been an increasing interest in plasmonic nanostructures, as they allow light confinement into sub-wavelength dimensions leading to enhanced light-matter interactions, which can be exploited to boost the linear and nonlinear optical response of organic molecules [1, 2].

Organo-metallic heterostructures display combinations of organic and inorganic properties [3]. Interesting effects have been observed such as shifts of the plasmon absorption resonance [4], modification of the Raman emission pattern [5] and spectral range of molecular fluorescence [6], hybridization between the plasmon mode and the exciton of the organic chromophore [7], and enhancement of the surface-enhanced Raman response under resonant illumination [8]. Not all these phenomena, especially those involving the nonlinear response of these hybrid systems, are fully understood. For example, the excitation of surface plasmons does not always lead to an enhanced nonlinear response, despite the fact that such excitation corresponds to a strong enhancement of the electric field at the metal surface, and the mechanisms underlying resonant surface-enhanced Raman spectroscopy are not known precisely.

This Master Thesis reports the results of an experimental and theoretical study performed on metallic nanoparticles covered with a thin organic film. We show that the nonlinear optical response of the organic dye is strongly affected by the vicinity of metallic structures. Second harmonic spectroscopy and interferometry measurements are carried out to extract both intensity and phase information. The results provide insight into the coupling of the molecular response to the light modes supported by the metal. A phenomenological model

of the observed features in terms of a dipolar coupling between two damped anharmonic oscillators is proposed.

2. Description of the techniques and experimental setup

Nonlinear optical phenomena occur when the response of a material to an applied optical field does not depend linearly upon the field strength. The polarization field inside the material can be expanded as a series of powers of the applied field as:

$$P(t) = \chi^{(1)}E(t) + \chi^{(2)}E(t)E(t) + \ldots \equiv P^{(1)}(t) + P^{(2)}(t) + \ldots \tag{1}$$

where $P^{(1)}(t)$ corresponds to the linear polarization and $P^{(2)}(t)$ to the second-order nonlinear polarization. The nonlinear polarization acts as a source of electromagnetic radiation at new frequencies which are not present in the applied field.

The simplest second-order nonlinear process is second harmonic (SH) generation, in which an applied field oscillating at ω is partially converted into a frequency-doubled field oscillating at 2ω. Since this is a coherent process, both intensity and phase information are contained in the 2ω field, which can be measured to obtain valuable information about the systems used as source of second harmonic light, as discussed in the following sections.

2.1. Second Harmonic Spectroscopy

Assuming only an electronic contribution, the polarization field is given by the density of microscopic dipoles induced in the material, or: $P = Nex$, where x represents the electronic response to the external electric field. The linear and quadratic parts of such response can be described by a simple model of an electron in an anharmonic potential well [9]. The corresponding equation of motion is:

$$\ddot{x} + \gamma\dot{x} + \omega_0^2 x + Dx^2 = \frac{eE_0}{2m}\left(e^{i\omega t} + e^{-i\omega t}\right) \tag{2}$$

where $x(t)$ is the displacement of the electron from its equilibrium position, mDx^2 is the anharmonic restoring force, γ is the damping term, and the driving electrical field $E_0\cos(\omega t)$ is written in its exponential form. The solution of Equation (2) has the form:

$$x(t) = q_1 e^{i\omega t} + q_2 e^{2i\omega t} + c.c. \tag{3}$$

The first term gives rise to the linear polarization $P^{(1)} = Ne\left(q_1 e^{i\omega t}\right)$, while the second term corresponds to the nonlinear polarization at 2ω, $P^{(2)} = Ne\left(q_2 e^{2i\omega t}\right)$. It is easily shown [9] that q_2 is given by:

$$q_2 = -\frac{De^2 E_0^2}{2m^2\left(\omega_0^2 - \omega^2 + i2\gamma\omega\right)^2\left(\omega_0^2 - 4\omega^2 + i2\gamma\omega\right)} \tag{4}$$

This description is particularly useful to explain second harmonic generation from absorbing (resonant) species such as organic chromophores and metallic nanoparticles. Looking at Equation (4), one sees that the polarization at 2ω has two resonances, the first when the photon energy is resonant with the absorption maximum, *i.e.* at $\omega = \omega_0$; and the second when the energy of two photons matches the maximum of absorption, at $2\omega = \omega_0$. It can be shown that the latter resonance is accompanied by a change of π in the phase of the generated SH light (see section 3 and Refs.[10]). The resonance at $\omega = \omega_0$ is not normally measured in second harmonic generation as the strong linear absorption hinders the nonlinear response.

The intensity of the generated SH light, which is given by:

$$I \propto |PP^*|^2 \Rightarrow I(2\omega) \propto |P^{(2)}P^{(2)*}|^2 \tag{5}$$

also has a resonance near the two-photon absorption threshold. The setup used to measure the second harmonic intensity as a function of the frequency is shown in figure 1.
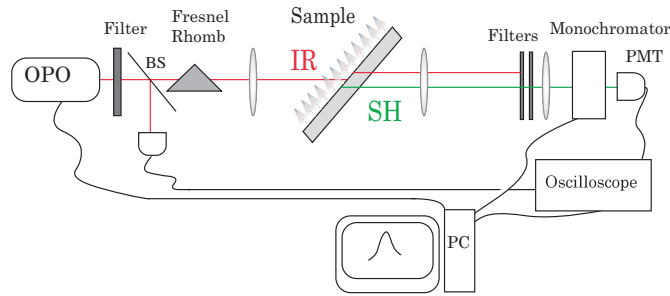
Figure 1. Schematic of the setup used for second harmonic spectroscopy.

The organic molecule used for the experiments is a dye called crystal violet (CV), which gives a relatively large $\chi^{(2)}$ (see eq.(1)). The metallic nanostructures employed are silver (Ag) nanoparticles, as they feature localized plasmon modes clearly separated from the absorption band of the dye.

In order to deposit the nanoparticles onto the glass substrates, two methods are employed. In the first method, a solution of polyvinylpyrrolidone-coated nanoparticles dispersed in 1,2-propandiol is spincasted onto a microscope glass slide and later annealed to about 450 K to desorb the polymer. The second approach consists in functionalizing the glass substrates with silanes (3-(aminopropyl)-triethoxysilane), whose amino groups favour the immobilization of the nanoparticles. The silanized substrates are immersed in a water suspension of monodispersed silver nanoparticles of 10 nm size. The adherence of the dye is easily achieved by simple immersion of the substrate into a 8×10^{-4} M CV solution in 1-propanol. After leaving the substrate immersed in solution for a few minutes, it is retrieved at constant speed of 0.3 mm/s. One side of the microscope slide is then cleaned to avoid second harmonic interferences between the two sides of the same substrate [11].

The light used for SH generation experiments comes from an optical parametric oscillator (OPO) pumped by a Q-switched Nd:YAG laser operating at 10 Hz. The idler beam from the OPO, whose wavelength is tuned between 750 and 1250 nm during the experiments, is passed through a filter to get rid of residual UV and visible light. The reflection off a clean glass slide is used as a trigger for the detection of the second harmonic signal. A Fresnel rhomb is used to rotate the beam polarization to p-polarization, which maximizes the second harmonic generation from the sample. A telescope system formed by two lenses of 20 cm focal length is employed to focus the incoming radiation onto the sample, which is positioned with the substrate normal at 45º with respect the laser beam. After filtering out the fundamental beam, the second harmonic light is focused into a monochromator by a 10 cm lens. The signal is detected by a photomultiplier tube at the monochromator output. The tuning of the OPO and the monochromator is controlled by computer, and the SH intensity is measured with an oscilloscope.

From intensity measurements at different wavelengths spectra are obtained in which the SH resonances can be observed. An urea sample positioned right after the first 20 cm lens is used to obtain a reference curve for the normalization of the measured spectra.
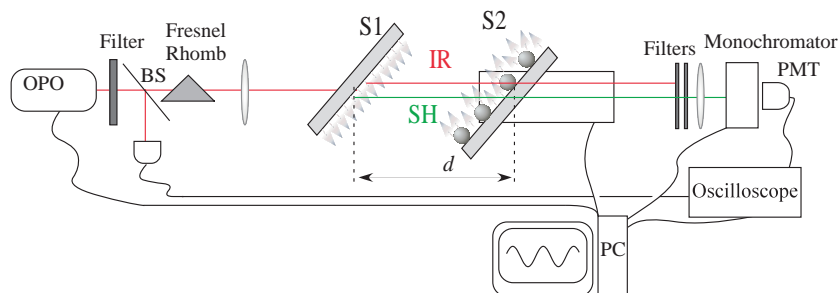
2.2. Second Harmonic Interferometry

As explained before, SH generation is a parametric nonlinear process from which both intensity and phase information can be extracted [12]. From the phase of the SH signal, the relative phase between the SH field and the (square of) fundamental beam at the moment of generation can be extrapolated, which yields information about the generation process.

In the second harmonic spectroscopy experiments described so far, phase information is necessary lost. However, it is possible to implement interferometric tools which exploit the relative dephasing between the fundamental and the SH beam propagating in dispersive media. The interferometric technique used here is based on the generation of second harmonic light by two consecutive nonlinear sources. Generation from the second source occurs with the presence of the second harmonic field coming from the first. The total SH intensity after the second source depends on the relative phases of the fundamental beam and the SH beam. If these two fields reach the second source with the proper phase, further generation of second harmonic light will occur, whereas a phase mismatch will lead to a backconversion from second harmonic to fundamental [13].

By varying the distance between the two sources, the optical path difference between the fundamental and SH beams is changed. Due to the wavelength dependence of the phase velocity in the medium embedding the sources (air), the fundamental and the second harmonic will reach the second source with different phases. As a consequence, the intensity after the second source will depend sinusoidally upon the distance between the sources. This results in an interferogram from which a frequency and a phase are obtained. The frequency is a measure of the dispersion of light in the medium embedding them [14].

The interferograms are acquired with the setup shown in figure 2. The experimental setup is very similar to the one used in section 2.1. The filtered idler beam passes through the Fresnel rhomb and encounters a 100 cm lens. The purpose of this lens is to obtain a weakly focused beam with a long Rayleigh range in which the energy density is approximately constant. The first nonlinear source (S1) is mounted on a fixed stage, whereas the second (S2) is placed on a motorized translation stage. The rest of the setup is identical to that described in section 2.1.

Figure 2. Schematic of the setup used for second harmonic interferometry.

The interferograms are recorded by displacing the second sample over a total distance of 310 nm along the beam direction, in steps of 5 mm for each wavelength from 750 until 1250 nm. The position of the second sample and data acquisition are controlled by computer using a simple LabVIEW® routine.

Due to the resonant character of $\chi^{(2)}$, the 2ω polarization is dephased with respect the square of the fundamental field, and this dephasing (or retardation) depends on the frequency. The measured phase represents the difference between the phase retardation at the first source and that at the second source.

2.3. Optical Coupling Model

We can extend the simple model presented in section 2.1 to describe SH generation from a nonlinear molecule in the vicinity of a metal nanoparticle. As the size of these nonlinear sources are very small compared to the wavelengths of the light employed, they are usually modeled as point-like scatterers (dipoles) in theoretical calculations [15, 16]. The new model consists of two externally driven damped anharmonic oscillators whose oscillations are coupled. The

equations of motion for the two oscillators are written as:

$$\ddot{x} + \gamma_M \dot{x} + \omega_M^2 x = -\frac{a_M}{m} x^2 + \frac{e}{m} \left(E_P^{2\omega} + E^\omega \right) \tag{6}$$

$$\ddot{y} + \gamma_P \dot{y} + \omega_P^2 y = -\frac{a_P}{m} y^2 + \frac{e}{m} \left(E_M^{2\omega} + E^\omega \right) \tag{7}$$

where x and y are the electronic displacement for the molecule (M) and the nanoparticle (P), respectively. E^ω is the optical field of the incident fundamental light, and $E_j^{2\omega}$ is the field at 2ω generated by the nanoparticles or molecules. Finally, a_M and a_P are parameters that characterize the strength of the nonlinearity of the molecules and nanoparticles.

The expressions for the generated SH fields are :

$$E_M^{2\omega} = i\frac{k_z}{\varepsilon_0} P_{s,2\omega}^M = i\frac{k_z e}{\varepsilon_0} N_s^M x_{2\omega} \tag{8}$$

$$E_P^{2\omega} = i\frac{k_z}{\varepsilon_0} P_{s,2\omega}^P = i\frac{k_z e}{\varepsilon_0} N_s^P y_{2\omega} \tag{9}$$

in which N_s^j is the surface density for molecules (M) and nanoparticles (P), $x_{2\omega}$ and $y_{2\omega}$ are the electronic displacement at 2ω, and k_z is the modulus of the propagation vector in the z direction $k_z = 2\omega/c$. While the surface polarization at 2ω ($P_{s,2\omega}^M$) of the molecules comes uniquely from their nonlinear susceptibility, that of the nanoparticles ($P_{s,2\omega}^P$) has two contributions, the hyperpolarizability and the induced polarization of the metal sphere due to nearby dipoles.

Assuming that the applied field is sufficiently weak, the nonlinear terms will be smaller than the linear ones, and eqs. (6) and (7) can be solved perturbatively. Solving the equations keeping only the linear terms oscillating at ω, we get:

$$x_L = \frac{e}{m} \frac{E^\omega e^{-i\omega t}}{\left(\omega_M^2 - \omega^2 - i\gamma_M^2 \omega^2 \right)} \tag{10}$$

$$y_L = \frac{e}{m} \frac{E^\omega e^{-i\omega t}}{\left(\omega_P^2 - \omega^2 - i\gamma_P^2 \omega^2 \right)} \tag{11}$$

The solution at 2ω is found by substituting these expressions for the quadratic terms x^2 and y^2 in eqs. (6) and (7). Writing the generated fields at 2ω as $E_M = ib_P x_{2\omega}$ for the molecules and $E_P = ib_M y_{2\omega}$ for the nanoparticles, the equations for the nonlinear response at 2ω become:

$$\ddot{x} + \gamma_M \dot{x} + \omega_M^2 x = -\frac{a_M}{m} x_L^2 + ib_M y \tag{12}$$

$$\ddot{y} + \gamma_P \dot{x} + \omega_P^2 y = -\frac{a_P}{m} y_L^2 + ib_P x \tag{13}$$

The solutions are of the form of $x \sim A \exp(-i2\omega t)$ and $y \sim B \exp(-i2\omega t)$. Inserting this expressions into eqs.(12) and (13), we get:

$$A = -\left[\left(\frac{e}{m} \right)^2 \frac{E_\omega^2}{m} \right] \frac{a_M D_P(2\omega) D_M^{-2}(\omega) + ib_M a_P D_P^{-2}(\omega)}{D_P(2\omega) D_M(2\omega) + b_M b_P} \tag{14}$$

$$B = -\left[\left(\frac{e}{m} \right)^2 \frac{E_\omega^2}{m} \right] \frac{a_P D_M(2\omega) D_P^{-2}(\omega) + ib_P a_M D_M^{-2}(\omega)}{D_P(2\omega) D_M(2\omega) + b_M b_P} \tag{15}$$

$$D_j(\omega) = \omega_j^2 - \omega^2 - i\gamma_j \omega; \quad j = M, P \tag{16}$$

Looking at the equations for the amplitudes A and B, we see that they display resonances when the pump energy corresponds to the maximum linear absorption of both the molecules and the nanoparticles, *i.e.* at $\omega = \omega_M$ and $\omega = \omega_P$. But more importantly for our experiments, near the two-photon absorption maxima coupled resonances appear which are shifted in frequency with respect to those of the isolated components. The spectral position of these coupled resonances depend on the relative strength of the nonlinearity (a_j) and on the product of the radiation efficiency at 2ω (b_j).

3. Results and Discussion

Before discussing the experiments performed on the coupled molecule-nanoparticle system, we report preliminary phase and intensity measurements carried out to test the applicability of the methods described in sections 2.1 and 2.2.

3.1. Experiment on the separate subsystems

Figure 3(a) shows examples of interferograms acquired at two fundamental wavelengths using two identical samples of crystal violet as sources. The distance d between the two sources is measured in millimeters, and the signal intensity is normalized between 0 and 1. These interferograms display little or no intensity variations, which demonstrates that the pump energy density remains constant over the hole distance covered by the second sample. The interferograms have been fitted with the function:

$$I(d) = I_0 + a\sin(f \times d + \varphi) \tag{17}$$

It can be seen from figure 3(a) that the quality of the fit is rather good. From the fits of several interferograms at different pump energy the wavelength dependence of the frequency f can be extracted , this is shown in figure 3(b) for the whole energy range probed. The value of φ corresponds to the phase of the sine function eq.(17) for $d = 0$, that is, when the two CV samples overlap. This value is shown in figure 3(c) for all probed wavelengths, and is a direct measure of the difference of the SH phase retardation (see section 2.2). As the two samples are equal they give rise to the same wavelength-dependent dephasing so that, the net phase difference is zero for each wavelength.
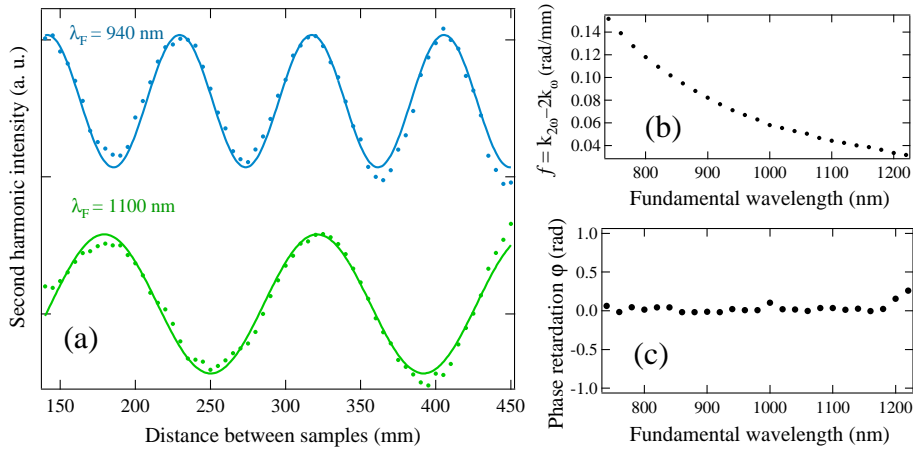
Figure 3. (a) SH interferograms using two CV samples as sources, acquired at fundamental wavelengths of λ=840 nm (blue, up line) and 1100 nm (green, bottom line) whose corresponding fits with eq.(17) are also shown. (b) Plot of the frequency of the sinusoidal modulation as a function of the fundamental wavelength. (c) Plots of the relative dephasing at $d = 0$ (φ) as a function of the fundamental wavelength.

The frequency f of the sinusoidal modulation corresponds to the wavevector mismatch between the fundamental and second harmonic fields [17]. Since the wave vector is proportional to the index of refraction, the frequency can be written as:

$$f = k_{2\omega} - 2k_\omega = \frac{4\pi}{\lambda}(n_{2\omega} - n_\omega) \tag{18}$$

We can therefore extract the difference in refractive index between the wavelength $\lambda/2$ (SH signal) and λ (fundamental beam) for air by multiplying the frequencies obtained by the corresponding fundamental wavelength times a constant. The resulting curve is in good

agreement with the dispersion of light in air [18].

Figure 4(a) displays the SH intensity versus fundamental wavelength for a thin film of silver nanoparticles obtained with the spin-coating method (see section 2.2). Next to it in figure 4(b), we show the phase obtained by SH interferometry experiments performed with the nanoparticle sample mounted on the fixed stage, and a crystal violet sample on the motorized stage.
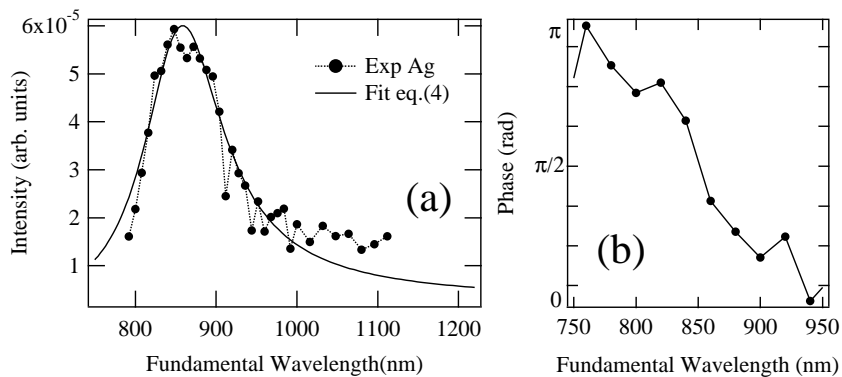
Figure 4. (a) Intensity of the SH signal for spincoated silver nanoparticles measured as a function of fundamental wavelength (filled circles), the fit of the eq.(4) is plotted for comparison (solid line). (b) Second harmonic phase of the same system displaying a phase shift of π across the resonance .

The spectrum of figure 4(a) displays a resonance at approximately $\lambda_{2\omega_0} = 850$ nm, as obtained by a fit of the experimental data using Equation (4). The plasmon absorption peak of the nanoparticle film, as measured by extinction spectroscopy, is centered at $\lambda_{\omega_0} = 420$ nm which matches the second harmonic resonance.

Looking at the results for the SH phase shown in figure 4(b), we clearly see a shift of π in the region of the nanoparticle plasmon resonance in agreement with the predictions of the model presented in section 2.1 (eq.(4)). The interferograms could only be measured in the range of figure 4(b) since above 950 nm the second harmonic intensity generated by the nanoparticles was too low ad did not yield a clear contrast between maxima and minima.

3.2. Experiments on the coupled system

We have prepared two types of samples using the silanized substrates, one obtained by depositing only a molecular film, and the other anchoring the silver nanoparticles and then depositing the crystal violet. The second harmonic spectra of the two samples are shown in figure 5(a). The SH spectrum of the nanoparticles could no be measured as the density of immobilized nanoparticles was too low to generate enough second harmonic signal.

The spectrum of the crystal violet film has a peak at $\lambda_{2\omega_0} = 1060$ as measured by fitting the experimental data with Equation (4). This peak displays a very large blueshift (50 nm) in the presence of the nanoparticles. We can see in figure 5(b) that the extinction spectrum of the crystal violet sample exhibits two absorption bands, one at $\lambda_{\omega_0} = 530$ nm which is the one observed in the second harmonic spectra and another at 620 nm. The origin of the two bands in absorption is not precisely known [19]. Figure 5(b) also shows the extinction spectrum of the dye film deposited onto the immobilized nanoparticles. Another peak at 380 nm is observed, originated by the silver nanoparticles. This peak corresponds to the electric-quadrupole plasmon resonance [20]. The linear resonances of the dye remain unshifted, which shows that the effect of the optical coupling is only reflected in the second harmonic spectra, in
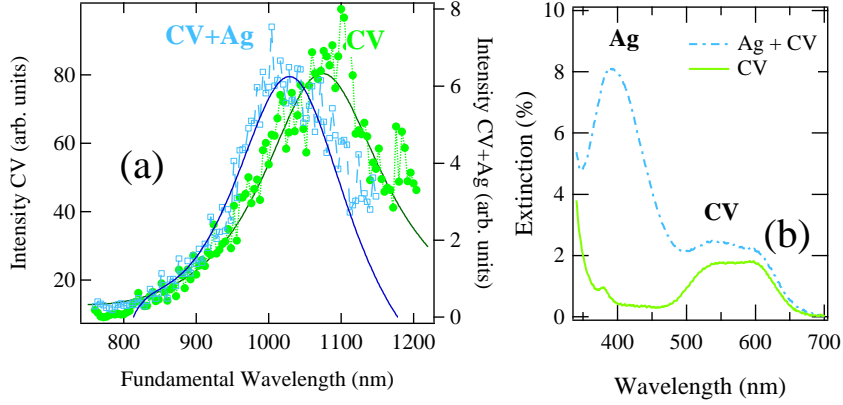
Figure 5. (a) SH spectrum of a CV film on a silanized substrate (green filled circles) and a CV film on immobilized Ag nanoparticles (blue empty squares). The calculated spectrum (solid line) is also plotted for both systems (b) Extinction spectra of the CV sample (green solid line) and the sample containing both CV and Ag nanoparticles (blue dashed and dotted line), after subtraction of the constant background at long wavelengths.

agreement with the predictions of the proposed model eqs.(10,11) and eqs.(14,15). By setting the resonances at $\lambda_{\omega 0}^{\mathrm{M}} = 530$ nm and $\lambda_{\omega 0}^{\mathrm{P}} = 380$ for molecules and nanoparticles respectively, we are able to reproduce rather well the experimental data with the model as it can be seen from figure 5(a). We note that the intensity of the second harmonic generated by the coupled system is smaller (right axis) than the signal generated by the dye alone (left axis). This is probably due to the fact that CV molecules adsorbed onto the nanoparticles have a random orientation while the ones sitting on a flat surface are ordered, so that the total intensity is higher.

We finally discuss the results obtained on CV adsorbed directly on a microscope glass slide and on the nanoparticle sample obtained by spin coating. The corresponding spectra are shown in figure 6(a).
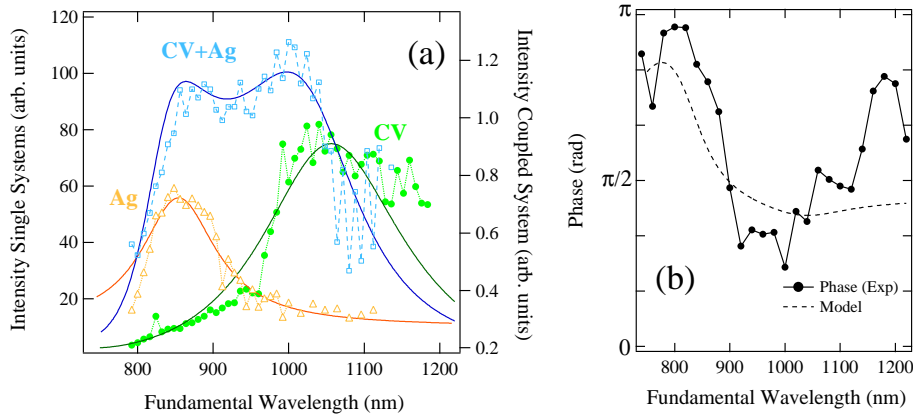
Figure 6. (a) SH intensity measurements for Ag nanoparticles (orange empty triangles) already shown in figure 4(a), CV (green filled circles) and the coupled system containing both Ag and CV (blue empty squares), the model is plotted for comparison (solid line). (b) Extrapolated phase of the coupled system (filled circles) extracted from interferograms, and the predicted phase with the model (dashed line).

The CV sample shows a peak around 1050 nm, albeit a bit less clear than that of figure 5(a) due to the more intense tail at long wavelengths. The second harmonic spectrum of the CV film on top of the spin-coated nanoparticles displays two peaks which are shifted with

respect to those of the nanoparticles or molecules alone. In the region of nanoparticle second harmonic generation, the observed peak displays a small redshift, whereas in the region of the dye resonance the peak is blueshifted by about 30 nm. With the model we are able to reproduce these asymmetric shifts by changing the radiation efficiencies b_j (see section 2.3). We therefore find that the maxima of second harmonic generation are shifted both when only the molecules generate and when molecules and nanoparticles generate together.

We carried out interferometry measurements with a crystal violet sample mounted on the fixed stage, and a sample of crystal violet deposited onto spincasted silver nanoparticles mounted on the translation stage. The measured phase difference is shown in figure 6(b). There are two major phase changes of π, one in the region of the nanoparticle resonance and the other in the region of the dye. With the model we are able to roughly reproduce the wavelength dependence of the phase by using the same parameters used for modeling the second harmonic spectra of the same system, shown in figure 6(a). As explained in section 2.2, the measured phase in figure 6(b) corresponds to the difference of the second harmonic phase retardation at the two samples. This is equivalent to calculate the phase of the total polarization of the coupled system and subtracting that of the isolated molecules (dashed line in figure 6(b)).

The first phase shift originates from the second harmonic resonance of the nanoparticles coupled to the dye. Since the nanoparticles are only present in one of the two samples used in the second harmonic interferometry measurements, we can expect a shift of π in the phase difference φ, similar to that observed in figure 4(b). On the contrary, the phase retardation due to the molecular resonance partially cancels out since the dye is present on both samples. Comparing the experimental data and the calculated phase, we see that the model predicts a less pronounced change of phase across the dye's resonance than that found experimentally. To avoid having to subtract phase retardations from two distinct resonant samples, we are planning to perform "absolute" phase measurements using a non resonant thin-film source of second harmonic, that would give second harmonic dephasing at all wavelengths.

4. Conclusions

The optical properties of plasmonic nanoparticles and organic molecules are known to be strongly modified when they are in close vicinity to each other. We have performed second harmonic (SH) spectroscopy and interferometry experiments on molecular films deposited on metallic nanoparticles with the aim of investigating the origin of these effects and their impact on the nonlinear optical response.

Silver nanoparticle samples on fused silica substrates were obtained either by spincoating of polymer-coated nanoparticles or by immobilization of monodispersed nanoparticles onto substrates functionalized with a silane monolayer. The first type of samples showed a strong electric-dipole plasmon resonance at 420 nm in extinction and generated a detectable SH signal peaked at the same wavelength. In the second class of samples only a weak electric-quadrupole plasmon resonance at 380 nm was observed, and the nanoparticle concentration was too low to give a measurable SH generation.

The SH spectrum of the organic dye was found to undergo a large blueshift in molecular films deposited on top of the metallic nanoparticles, while no shift was detected in the linear extinction spectra of the same samples. The blueshift was about 30 nm for the molecular film on top of the spincasted nanoparticles, and roughly 50 nm on top of the nanoparticles bonded to the silanes. This shows that the nonlinear response of the dye is strongly affected by the neighbouring metallic nanoparticles. In the first case also the nanoparticles generated a SH signal (only slightly redshifted), so that two peaks were observed in the SH spectrum. The phase of this SH light displayed a clear shift of π across the nanoparticle resonance and a smaller phase shift across the blueshifted resonance of the dye.

This purely nonlinear optical coupling could be modeled phenomenologically in terms of two damped anharmonic oscillators with coupled oscillations. With this simple model we were able to reproduce both the intensity and phase of the generated SH light, using the same set of parameters. Our findings might open the way to a new route for controlling light generation in hybrid systems.

Acknowledgments

References

[1] Horimoto N N, Imura K and Okamoto H 2008 *Chem. Phys. Lett.* **467** 105–9
[2] Ishifuji M, Mitsuishi M and Miyashita T 2009 *J. Am. Chem. Soc.* **131** 4418–24
[3] Agranovich V M, Basko D M, La Rocca G C and Bassani F 1998 *J. Phys.: Condens. Matter* **10** 9363–400
[4] Averitt R D, Sarkar D and Halas N J 1997 *Phys. Rev. Lett.* **78** 4217–20
[5] Shegai T, Li Z, Dadosh T, Zhang Z, Xu H and Haran G 2008 *PNAS* **105** 16448–53
[6] Ringler C, Schwemer A, Wunderlich M, Nichtl A, Kürzinger K, Klar T A and Feldman J 2008 *Phys. Rev. Lett.* **100** 203002
[7] Wurtz G A, Evans P R, Hendren W, Atkinson R, Dickson Wayne, Pollard R and Zayats A V 2007 *Nano Lett.* **5** 1297–303
[8] McFarland A D, Young M A, Dieringer J A and Van Duyne R P 2005 *J. Phys. Chem.* **109** 11279–85
[9] Yariv A 1975 *Quantum Electronics* (USA : John Wiley & Sons) 2nd Ed
[10] Heinz T F, Tom H W K and Shen Y R 1983 *Phys. Rev. A* **28** 1883–5
[11] Stolle R, Marowsky G, Schwarzberg E and Berkovic 1996 *J. Appl. Phys. B* **63** 491–8
[12] Boyd R W 2003 *Nonlinear Optics* (USA: Academic Press) 2nd Ed
[13] Botey M, Martorell J, Trull J and Vilaseca R 200 *Opt. Lett.* **25** 1177–9
[14] Macovez R, Mariano M and Martorell J 2009 *Submitted*
[15] Wiederrecht G P, Wurtz G A and Hranisavljevic J 2004 *Nano Lett.* **4** 2121–5
[16] Myers Kelley A 2007 *Nano Lett.* **7** 3235–40
[17] Dolova T V, Schuhmacher R, Marowsky G, Fedyanin A A and Aktispetrov O A 2002 *Appl. Phys. B* **74** 653–9
[18] Bönsch G and Potulski E 1998 *Metrologia* **35** 133–9
[19] Lovell S, Marquardt B J and Kahr B 1999 *J. Chem. Soc., Perkin Trans. 2* 2241–7
[20] Jensen T, Kelly L, Lazarides A and Schatz G C 1999 *J. Cluster. Sci.* **10** 295–317